IIETA International Information and Engineering Technology Association
Advancing the World of Information and Engineering

Ingénierie des Systèmes d'Information
Vol. 30, No. 10, October, 2025, pp. 2625-2633
Journal homepage: http://iieta.org/journals/isi

Development of the Histogram of Oriented Gradients Method for Feature Extraction in Welding Defect Detection

Okta Veza[1*], Yuhandri[2], Sumijan[2]

[1] Faculty of Science and Technology, Ibnu Sina University, Batam 29432, Indonesia
[2] Department of Information Technology, Universitas Putra Indonesia YPTK, West Sumatra 25221, Indonesia

Corresponding Author Email: okta@uis.ac.id

https://doi.org/10.18280/isi.301009

Received: 6 August 2025
Revised: 12 October 2025
Accepted: 20 October 2025
Available online: 31 October 2025

Keywords:
welding defect detection, TAHOG, gradient angle decomposition, X-ray imaging, feature extraction, automated inspection

ABSTRACT

Welding defect detection is a critical component of quality inspection systems in the manufacturing industry. This study proposes the Trigonometry and Adaptive Histogram of Oriented Gradients (TAHOG) method as an extension of the conventional Histogram of Oriented Gradients (HOG), incorporating logarithmic and adaptive exponential functions in the gradient angle decomposition process to enhance feature extraction sensitivity in X-ray welding images. The methodology involves preprocessing, weld region segmentation, and feature extraction using both HOG and TAHOG on a dataset of 500 X-ray images, divided into training and testing sets. Comparatively, TAHOG demonstrates superior performance in detecting defect quantity, orientation, and defect area. The HOG method yields an average defect ratio of 7.58%, lower than 11.85% obtained using TAHOG, and tends to generate fragmented defect mappings, leading to less representative damage characterization. In contrast, TAHOG maintains higher sensitivity to variations in defect structure and orientation. Experimental results indicate that TAHOG achieves 99.77% accuracy, 100% precision, 99.54% recall, 99.77% F1-score, and 100% specificity, reflecting an optimal balance between defect detection capability and avoidance of misclassification in non-defective regions. Therefore, TAHOG effectively addresses the limitations of HOG in detecting low-intensity defects and contributes significantly to improving the accuracy and reliability of automated welding inspection systems in industrial environments.

1. INTRODUCTION

TAHOG is a method derived from the Histogram of Oriented Gradients (HOG), specifically developed to enhance the effectiveness of visual feature extraction in image-based welding defect detection. As the demand for automated inspection systems in the manufacturing industry increases, visual detection of welding defects has become essential to ensure the quality of weld joints while minimizing the risk of structural failures [1]. Welding itself is the process of joining materials using heat or pressure, where the quality of the joint strongly depends on the process parameters and techniques employed [2]. Therefore, good weld joints—defined as those free from defects—are a key factor in improving the strength and reliability of welded structures. Previous studies have demonstrated that variations in welding parameters significantly affect the strength of dissimilar metal joints, where changes in visual patterns of the welds can be extracted using gradient orientation approaches such as HOG, thus making visual methods increasingly relevant in modern inspection systems [3].

HOG has proven effective in extracting critical features in welding areas for both classification and surface defect detection. Yu et al. [4] developed a butt weld penetration monitoring system based on infrared sensors and an improved HOG algorithm, allowing stable penetration detection even in the presence of arc light disturbances during the welding process. The integration of HOG with convolutional neural networks (CNN) has also been shown to improve classification accuracy, as demonstrated by Zhang et al. [5] in ship object recognition using SAR imagery. Optimization of HOG parameters, such as cell size and gradient orientation, has been conducted to improve visual detection performance in industrial settings [6].

The combination of HOG with deep learning has also been proven to increase welding defect detection accuracy by over 15% and to enhance sensitivity to finer surface defects [7]. Furthermore, feature fusion techniques that combine HOG with other methods have effectively increased classification accuracy in small-sized weld defect image datasets [8]. In visual sensor-based surface defect detection, the implementation of HOG–SVM methods has demonstrated high accuracy and processing efficiency for various types of defects [9]. Comparisons of feature extraction methods have revealed that HOG achieved the highest classification accuracy, up to 95%, on small radiographic datasets [10]. The addition of data augmentation and integration of CNN and HOG features has also been shown to improve multiclass

classification accuracy to an average of 92% [11].

Furthermore, visual inspection methods utilizing gradient features such as HOG combined with deep learning have resulted in highly accurate automated detection [12]. HOG is also recognized as an important baseline for defect recognition from X-ray images, even when compared to the latest deep learning methods [13]. Its application in visual infrastructure such as pipelines and utility networks, has also proven effective [14]. Other innovations, such as HOG–Poly–SVM for defect detection on phased-array ultrasonic TFM images, have achieved accuracy rates exceeding 93% [15]. Integration of HOG into simple CNN architectures also provides significant improvements in precision and recall [16], and enables the identification of various types of weld defects on radiographic images with competitive performance [17].

The application of HOG–Linear–SVM to ultrasonic NDT images for minor flaw detection can achieve accuracies up to 98% [18], while HOG–Poly–SVM shows better performance on ultrasonic phased array pipeline datasets [19]. Additionally, the combination of visual attention mechanisms and HOG features in deep learning models enhances precision and provides interpretability for radiographic defect detection results [20]. The application of these methods has also expanded to nondestructive inspection of complex heat sink fin welds using infrared images and deep learning [21], as well as automated weld penetration measurement based on dual-band imaging and neural networks with HOG features [22].

Beyond welding, HOG is also adopted for real-time human tracking systems based on Faster R-CNN and metaheuristic optimization [23], as well as for automated surface defect detection using laser visual sensors with HOG–SVM, achieving identification accuracy of up to 97.86%. Building upon these prior studies, TAHOG is expected to make a significant contribution to improving the accuracy, efficiency, and reliability of automated welding defect detection. This innovation offers substantial benefits for the industrial sector, particularly in accelerating inspection processes, reducing human error, and ensuring optimal manufacturing quality, thereby supporting efficiency, safety, and competitiveness in the modern industrial era.

2. PROPOSED SYSTEM

This section describes the proposed feature extraction framework designed to enhance welding defect detection performance. The TAHOG method is introduced as an extended development of the conventional Histogram of Oriented Gradients (HOG) approach. In this study, the standard HOG method is retained as a baseline reference to enable a fair and measurable comparison of feature extraction performance. While HOG computes gradient orientation features using a fixed cell–block structure, TAHOG integrates an adaptive trigonometric logarithmic gradient decomposition mechanism to improve sensitivity to low contrast defect patterns and fine structural details in X-ray welding images.

2.1 Block and cell size

In the conventional HOG descriptor, the image is partitioned into spatial regions called *cells* of size 16×16 pixels, and several adjacent cells are grouped into overlapping blocks to provide normalization against illumination differences. This cell-block configuration is retained in this study to ensure consistent representation and to maintain fairness in comparison. In TAHOG, the same cell and block sizes are preserved. However, unlike HOG, the gradient refinement is performed before histogram construction, allowing enhanced directional sensitivity prior to cell block aggregation.

2.2 Image gradient

The input RGB image is first converted into a grayscale representation to reduce computational complexity while preserving structural information. The horizontal and vertical gradients are then computed using discrete convolution operations as follows.

$$I_x = f(x,y) - f(x,y+2) \tag{1}$$

$$I_y = f(x,y) - f(x+2,y) \tag{2}$$

The gradient magnitude and orientation at each pixel are obtained using:

$$m(x,y) = \sqrt{I_x^{\,2} + I_y^{\,2}} \tag{3}$$

$$\theta(x,y) = tan^{-1}\frac{I_y}{I_x} \tag{4}$$

2.3 Bin orientation

For the conventional HOG method, each gradient orientation is assigned to one of nine orientation bins spanning 0° to 180° with 20° resolution per bin. The gradient magnitudes contribute to the histogram of each cell, forming the core orientation distribution representation. This histogram representation is later normalized across blocks to enhance robustness to local contrast variation.

2.4 Trigonometric vector decomposition

This stage performs an adaptive decomposition of the gradient contribution into two dominant orientation responses. Let G and θ denote the gradient magnitude and angle obtained from imgradientxy. Two reference orientations are defined at θ1=0◦ (horizontal) and θ2=90◦ (vertical). The gradient vector is projected toward these references using trigonometric weighting as follows:

$$G_1 = G \cdot \frac{\sin(\theta_2 - \theta)}{\sin(\theta_2 - \theta)\cos(\theta - \theta_1) + \sin(\theta - \theta_1)\cos(\theta_2 - \theta)} \tag{5}$$

$$G_2 = G \cdot \frac{\sin(\theta - \theta_1)}{\sin(\theta_2 - \theta)\cos(\theta - \theta_1) + \sin(\theta - \theta_1)\cos(\theta_2 - \theta)} \tag{6}$$

Trigonometric-Based

However, trigonometric projection alone remains sensitive to noise in low-contrast weld regions. Therefore, an adaptive logarithmic–exponential weighting is introduced to improve angular discriminability:

$$L1 = log(1 + e^{-\alpha|\ \theta - \theta 1|\ \beta}),\ L2 = log(1 + e^{-\alpha|\ \theta - \theta 2|\ \beta}) \quad (7)$$

where, α controls the sharpness of angular selectivity and β regulates smoothing. The logarithmic term suppresses noise in homogeneous regions, while the exponential term amplifies subtle angular variations, enabling the detection of fine and weak weld defects that are frequently lost under HOG's block-based averaging.

The final directional gradient maps are then computed as:

$$L_1 \begin{cases} G_1 = G \cdot \dfrac{L_1}{L_1 + L_2} \\ G_2 = G \cdot \dfrac{L_2}{L_1 + L_2} \end{cases} \quad (8)$$

Algorithmic and Exponential-Based

This pixel-wise adaptive projection preserves small discontinuities and crack-like patterns, thereby improving sensitivity to low-intensity defects that are typically smoothed out in traditional HOG cell–block normalization.

2.5 Block normalization

Block normalization is performed to minimize the impact of illumination and contrast variations, ensuring that the extracted TAHOG features remain stable under different image intensity conditions. The normalization process is expressed as:

$$V_n = \sqrt{\frac{v}{\|v\| + \varepsilon}} \quad (9)$$

To ensure a fair and unbiased performance comparison, both the conventional HOG and the proposed TAHOG method are designed to produce the same final feature dimensionality. For an input image of size 256×256 pixels, both methods yield a 9,216-dimensional feature vector. This equivalency in representation size guarantees that any observed performance improvements are attributed solely to the adaptive gradient decomposition mechanism introduced in TAHOG, rather than to differences in feature dimensionality or descriptor scale. Accordingly, the enhancement reported in this study reflects the intrinsic effect of the trigonometric logarithmic gradient refinement, independent of classifier influence or feature length expansion.

Here is the framework illustrating the development from HOG to the proposed TAHOG method:

The framework presented in Figure 1 illustrates the workflow of the proposed welding defect detection system in X-ray images. The process begins with image acquisition, followed by a preprocessing stage aimed at enhancing structural detail and suppressing irrelevant visual variations. This stage includes noise reduction, contrast stretching, local enhancement, intensity normalization, and high-pass filtering to emphasize gradient transitions and fine surface irregularities.

After preprocessing, the image undergoes segmentation to isolate the weld seam as the primary region of interest. Feature extraction is then performed using two comparative approaches, namely the conventional Histogram of Oriented Gradients (HOG) and the proposed Trigonometry-Adapted Histogram of Oriented Gradients (TAHOG). In HOG, gradient descriptors are computed and aggregated within a fixed cell–block structure. In contrast, TAHOG introduces an adaptive trigonometric–logarithmic gradient decomposition mechanism designed to preserve low-intensity directional variations that are typically diminished by cell–block normalization in HOG.

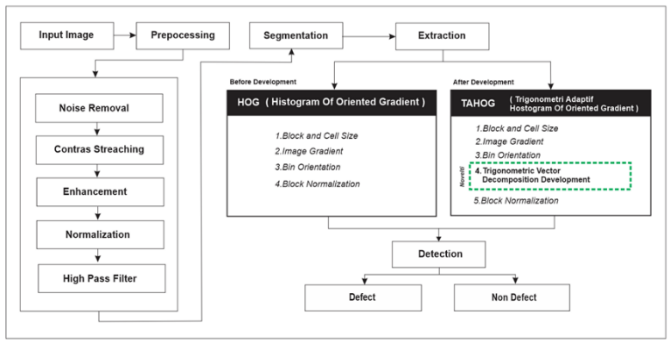

Figure 1. TAHOG processing pipeline for welding defect detection

The extracted features are subsequently analyzed to identify discontinuities, texture distortions, or directional irregularities indicative of weld defects. It should be noted that this study is focused on evaluating improvements at the feature extraction level, and therefore does not employ an external classifier. Accordingly, the performance comparison between HOG and TAHOG reflects the intrinsic contribution of the proposed gradient decomposition mechanism, rather than the influence of classifier parameters or behavior.

It is important to clarify that the objective of this study is to assess the improvement at the feature extraction stage. Therefore, no external classifier is employed in the detection pipeline. This ensures that the performance comparison between HOG and TAHOG reflects the intrinsic enhancement introduced by the proposed gradient decomposition mechanism, independent of classifier behavior or training bias.

3. RESULTS AND DISCUSSION

This section emphasizes the need for an effective feature extraction method to enhance detection accuracy. The TAHOG method, an adaptive extension of HOG, is used for its improved sensitivity in capturing directional and structural image features. The process starts by importing labeled images (welding1 to welding10) to train the system for input recognition, as illustrated in Figure 2.

The dataset includes three primary weld defect types frequently encountered in radiographic inspection, as classified under ISO 6520-1 (Classification of Geometric Imperfections in Metallic Materials – Welds): elongated defects (100-series), round or porosity defects (200-series), and lack-of-fusion defects (401). Elongated defects manifest as stretched or linear discontinuities along the weld seam, round defects appear as circular voids resulting from trapped gas, and lack-of-fusion defects arise when the filler metal fails to adequately bond with the base material. These defect types exhibit distinct gradient and texture characteristics, making them appropriate for performance evaluation using the proposed TAHOG feature extraction method.

Noise Removal is the first preprocessing step in welding X-

ray images, removing noise to improve clarity and highlight defect structures, as illustrated in Figure 3.

Contrast stretching enhances the pixel intensity distribution in welding X-ray images, thereby improving visual contrast and facilitating clearer detection of weld lines and defect regions, as illustrated in Figure 4.

Contrast Enhancement enhances intensity differences in welding X-ray images to reveal subtle defects, enabling more accurate weld quality assessment, as illustrated in Figure 5.

Normalization equalizes the intensity distribution in welding X-ray images to minimize lighting variations, thereby improving the detectability of weld defects, as illustrated in Figure 6.

High-pass filter highlights fine details in welding X-ray images, making weld defects clearer and easier to detect, as illustrated in Figure 7.

Segmentation separates the weld area from the background in a black-and-white format, facilitating defect detection and further analysis, as illustrated in Figure 8.

Segmentation extracts the weld region, HOG highlights potential defects, and TAHOG offers clearer and more sensitive defect localization, as illustrated in Figure 9.

No	Images	Description
1		Welding.1
2	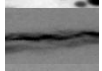	Welding.2
3		Welding.3
4	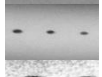	Welding.4
5	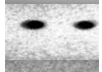	Welding.5
6	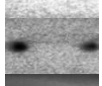	Welding.6
7		Welding.7
8		Welding.8
9		Welding.9
10		Welding.10

Figure 2. Initialization of the welding image dataset, labeled sequentially from Welding.1 To Welding.10

No	Description	Images	Noise Removal
1	Welding.1		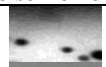
2	Welding.2	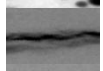	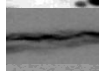
3	Welding.3		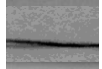
4	Welding.4	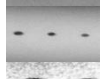	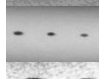
5	Welding.5		
6	Welding.6	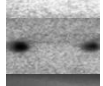	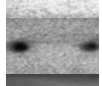
7	Welding.7		
8	Welding.8		
9	Welding.9		
10	Welding.10		

Figure 3. Welding X-ray images before and after noise removal

No	Description	Noise Removal	Contras Streching
1	Welding.1	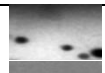	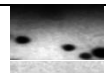
2	Welding.2		
3	Welding.3	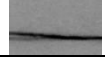	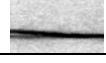

No	Description	Noise Removal	Contras Streching
4	Welding.4	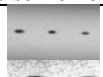	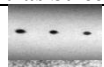
5	Welding.5		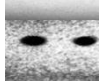
6	Welding.6	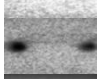	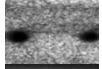
7	Welding.7		
8	Welding.8		
9	Welding.9		
10	Welding.10		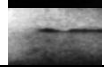

Figure 4. Welding X-ray images after noise removal and contrast stretching

No	Description	Contras Streching	Enhancement
1	Welding.1		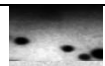
2	Welding.2		
3	Welding.3	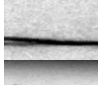	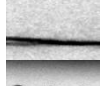
4	Welding.4	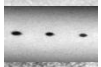	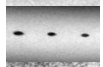
5	Welding.5	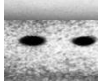	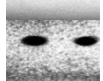
6	Welding.6	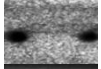	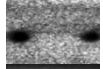
7	Welding.7		
8	Welding.8		
9	Welding.9		
10	Welding.10		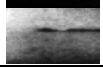

Figure 5. Welding X-ray images after contrast stretching and enhancement

No	Description	Enhancement	Normalization
1	Welding.1	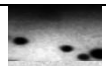	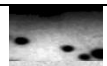
2	Welding.2		
3	Welding.3	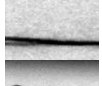	
4	Welding.4		
5	Welding.5		
6	Welding.6		
7	Welding.7		
8	Welding.8		
9	Welding.9		
10	Welding.10		

Figure 6. Welding X-ray images after enhancement and normalization

No	Description	Normalization	Highpass Filter
1	Welding.1		

No	Description	Normalization	Highpass Filter
2	Welding.2	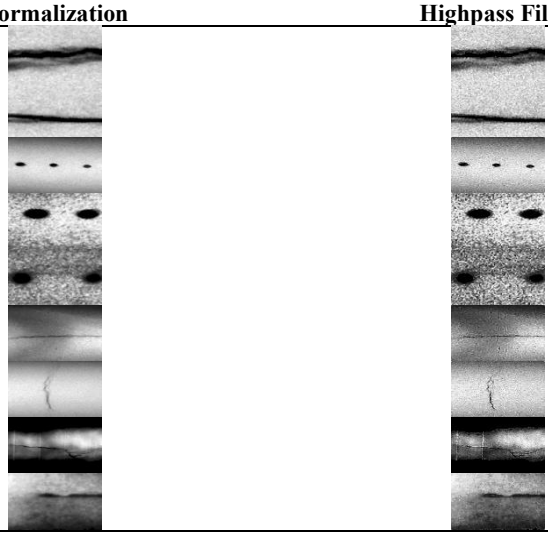	
3	Welding.3		
4	Welding.4		
5	Welding.5		
6	Welding.6		
7	Welding.7		
8	Welding.8		
9	Welding.9		
10	Welding.10		

Figure 7. Welding X-ray images after normalization and high pass filter

No	Description	Highpass Filter	Segmentation
1	Welding.1	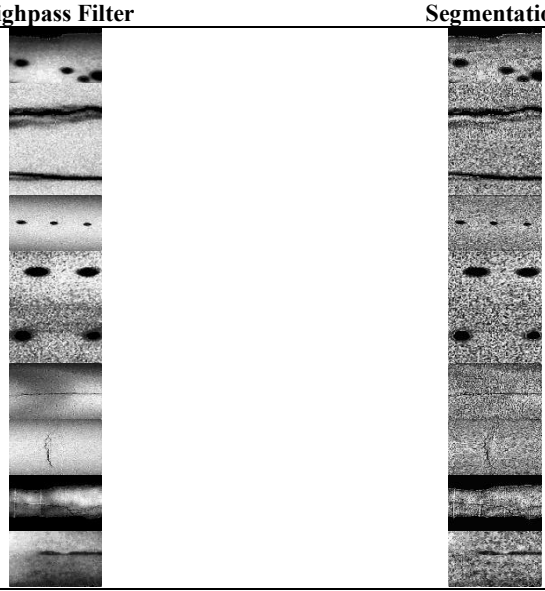	
2	Welding.2		
3	Welding.3		
4	Welding.4		
5	Welding.5		
6	Welding.6		
7	Welding.7		
8	Welding.8		
9	Welding.9		
10	Welding.10		

Figure 8. Welding X-ray images after high pass filter and segmentation

No	Description	Segmentation	Hog	TAHOG
1	Welding.1	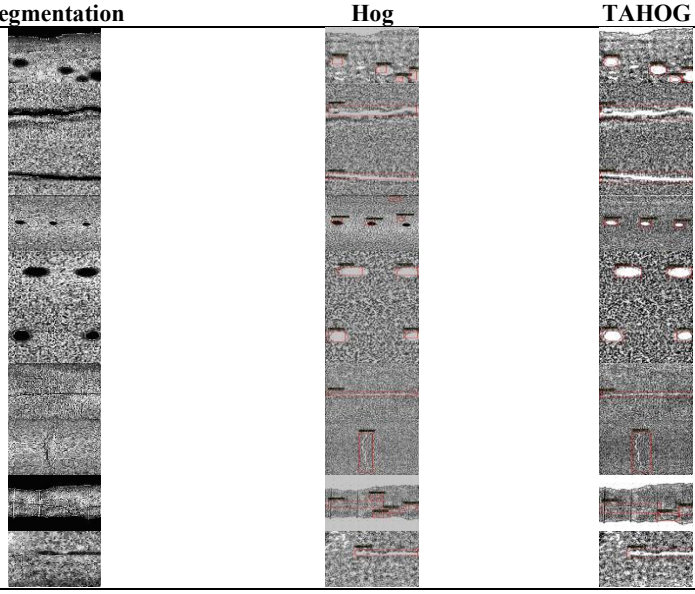		
2	Welding.2			
3	Welding.3			
4	Welding.4			
5	Welding.5			
6	Welding.6			
7	Welding.7			
8	Welding.8			
9	Welding.9			
10	Welding.10			

Figure 9. Visualization of segmentation and welding defect detection utilizing HOG and TAHOG methods

Table 1. Processing results obtained using HOG

HOG					
Number of Defects	**Horizontal Detection (G1)**	**Vertical Detection (G2)**	**Total Defect Area**	**Weld Seam Area**	**Defect Ratio**
4	2	2	1920	51529	3.73%
1	0	1	8320	51529	16.15%
1	0	1	4800	51529	9.32%
4	2	2	1280	51529	2.48%
2	0	2	3328	51529	6.46%
2	1	1	2368	51529	4.60%
1	0	1	3328	51529	6.46%
1	1	0	4864	51529	9.44%
5	0	5	5376	51529	10.43%
1	0	1	3456	51529	6.71%

Table 2. Processing results obtained using TAHOG

TAHOG					
Number of Defects	**Horizontal Detection (G1)**	**Vertical Detection (G2)**	**Total Defect Area**	**Weld Seam Area**	**Defect Ratio**
4	1	3	4402	51529	8.54%
1	1	0	12150	51529	23.58%
1	0	1	8697	51529	16.88%
3	1	2	2093	51529	4.06%
2	1	1	5331	51529	10.35%
2	2	0	4047	51529	7.85%
1	1	0	4950	51529	9.61%
1	0	1	7040	51529	13.66%
3	2	1	6940	51529	13.47%
1	1	0	5406	51529	10.49%

The following table presents the performance comparison between HOG and TAHOG in this study. For greater clarity, the processing results obtained using the HOG method are provided in Table 1.

The results obtained from the processing using the TAHOG method are presented in Table 2.

Based on the comparison table, the TAHOG method outperforms HOG in detecting welding defects, offering more realistic defect ratios and balanced directional detections (G1 and G2), indicating higher sensitivity and accuracy under complex image conditions. This is further illustrated in the graph below.

The following is a comparison between HOG and TAHOG, showing that TAHOG provides more accurate defect detection with higher sensitivity to gradient variations and image complexity.

TAHOG consistently demonstrates higher sensitivity compared to HOG. TAHOG produces a larger average defect ratio of 11.85% compared to 7.58% obtained using HOG. Although the number of detected defects is sometimes equal or slightly lower, TAHOG merges fragmented regions into unified objects and maps a wider defect area, resulting in a more representative depiction of weld damage severity. The G1–G2 directional patterns are also more adaptive, frequently switching dominant orientations, indicating strong robustness to variations in defect direction. In practical terms, this confirms the superiority of TAHOG in capturing subtle or low-contrast defects and providing a more detailed quantification of weld damage than the conventional HOG method.

The confusion matrix in Figure 10 illustrates the performance of the model on a testing dataset consisting of 500 welding X-ray images. The model successfully classified defective and non-defective regions, yielding only three false negatives and no false positives. Based on this configuration, the model achieved an accuracy of 99.77%, 100% precision for the defect class, 99.54% recall, 99.77% F1-score, 100% specificity, and 99.77% balanced accuracy. These results demonstrate both high sensitivity and perfect specificity, indicating that the proposed TAHOG method is highly reliable for welding quality inspection, with a minimal risk of false defect detection and strong suitability for real-time industrial implementation.

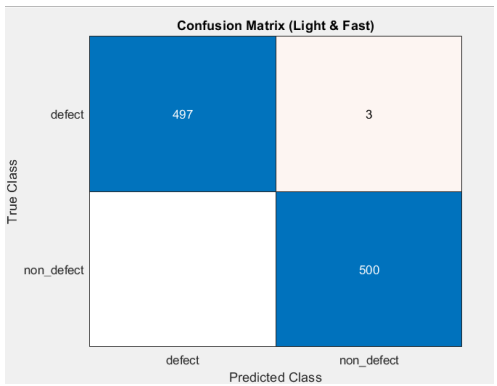

Figure 10. Confusion matrix

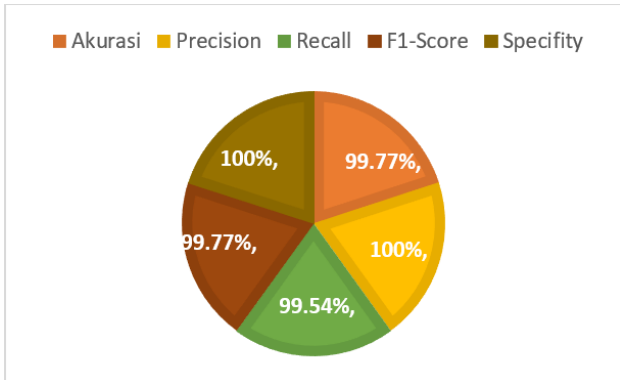

Figure 11. Performance evaluation diagram

The diagram in Figure 11 illustrates the performance of the TAHOG-based welding defect detection system evaluated using five standard metrics: accuracy, precision, recall, F1-score, and specificity. The experimental results indicate that the system achieves an accuracy of 99.77%, reflecting a very low overall misclassification rate. A precision value of 100% demonstrates that all defect predictions correspond to actual defects, with no false positive occurrences.

Meanwhile, a recall of 99.54% indicates that nearly all existing defects in the test images were successfully detected, with only a minimal number of false negatives. The F1-score of 99.77% reveals an optimal balance between precision and recall. Moreover, a specificity value of 100% confirms the system's ability to accurately identify non-defect regions without false detections.

Overall, these results affirm that the proposed TAHOG method provides highly reliable, stable, and effective performance in detecting welding defects in X-ray images, making it well-suited for deployment in real-world industrial quality inspection systems based on computer vision.

4. CONCLUSION

The development of the TAHOG method has proven effective in enhancing defect detection accuracy compared to the conventional HOG approach. By incorporating gradient angle decomposition based on adaptive logarithmic–exponential functions, TAHOG provides higher sensitivity to variations in defect orientation and low-intensity structural details within welding X-ray images. Additionally, TAHOG demonstrates the ability to detect a greater number of defects with more balanced directional responses in both horizontal and vertical orientations, thereby improving the overall coverage of automated inspection. Furthermore, TAHOG consistently delivers more accurate estimations of defect area and shape, resulting in more realistic defect characterization. These improvements originate solely from the adaptive gradient decomposition mechanism, as the feature vector dimensionality is maintained equal to that of HOG. Therefore, the proposed TAHOG method can be regarded as a reliable enhancement for feature extraction in welding inspection systems. However, this study has certain limitations that should be acknowledged. The research focuses only on the feature extraction stage and does not involve the use of advanced classification models such as convolutional neural networks (CNN) or other deep learning architectures. As a result, the performance comparison is limited to the classical HOG baseline and does not yet reflect competitiveness against modern end-to-end automated detection frameworks. Future work should integrate the TAHOG descriptor with deep learning-based classifiers and evaluate performance across larger and more diverse industrial datasets to validate its robustness in real-world inspection conditions.

REFERENCES

[1] Hu, D., Lü, B., Wang, J., Gao, X. (2023). Study on HOG-SVM detection method of weld surface defects using laser visual sensor. Transactions of the China Welding Institution, 44(1): 57-70. https://doi.org/10.12073/j.hjxb.20211231001

[2] Jiang, K., Wang, C., Ren, J., Li, Z., Zhou, G., Ma, T. (2025). Nondestructive inspection method of welding rate for heat sink fins with complex structure via infrared thermography principle and deep learning method. Expert Systems with Applications, 260: 125402. https://doi.org/10.1016/j.eswa.2024.125402

[3] Szusta, J., Derpeński, Ł., Karakaş, Ö., Tüzün, N., Dobrzański, S. (2023). Effect of welding process parameters on the strength of dissimilar joints of S355 and Strenx 700 steels used in the manufacture of agricultural machinery. Materials (Basel), 16(21): 6963. https://doi.org/10.3390/ma16216963

[4] Yu, R., Huang, Y., Peng, Y., Wang, K. (2023). Monitoring of butt weld penetration based on infrared sensing and improved histograms of oriented gradients. Journal of Materials Research and Technology, 22: 3280-3293. https://doi.org/10.1016/j.jmrt.2022.12.139

[5] Zhang, T., Zhang, X., Ke, X., Liu, C., Xu, X., Zhan, X., Wei, S. (2021). HOG-ShipCLSNet: A novel deep learning network with hog feature fusion for SAR ship classification. IEEE Transactions on Geoscience and Remote Sensing, 60: 1-22. https://doi.org/10.1109/TGRS.2021.3082759

[6] Nguyen, V.C., Le, H.T. D., Huynh, H.T. (2022). Hardware system implementation for human detection using HOG and SVM algorithm. arXiv preprint arXiv:2205.02689. https://doi.org/10.48550/arXiv.2205.02689

[7] Mohammed, A., Hussain, M. (2025). Advances and challenges in deep learning for automated welding defect detection: A technical survey. IEEE Access. https://doi.org/10.1109/ACCESS.2025.3574083

[8] Hou, W.H., Rao, L.L., Zhu, A.D., Zhang, D.S. (2022). Feature fusion for weld defect classification with small dataset. Journal of Sensors, 2022(1): 8088202. https://doi.org/10.1155/2022/8088202

[9] Palma-Ramírez, D., Ross-Veitía, B.D., Font-Ariosa, P., Espinel-Hernández, A., Sanchez-Roca, A., Carvajal-Fals, H., Hernández-Herrera, H. (2024). Deep convolutional neural network for weld defect classification in radiographic images. Heliyon, 10(9): e30590. https://doi.org/10.1016/j.heliyon.2024.e30590

[10] Molefe, M.E., Tapamo, J.R., Vilakazi, S.S. (2025). A comparative study of image processing and machine learning methods for classification of rail welding defects. Journal of Sensor and Actuator Networks, 14(3): 58. https://doi.org/10.3390/jsan14030058

[11] Say, D., Zidi, S., Qaisar, S.M., Krichen, M. (2023). Automated categorization of multiclass welding defects using the X-ray image augmentation and CNN. Sensors, 23: 6422. https://doi.org/10.3390/s23146422

[12] Spruck, A., Seiler, J., Roll, M., Dudziak, T., Eckstein, J., Kaup, A. (2020). Quality assurance of weld seams using laser triangulation imaging and deep neural networks. In 2020 IEEE International Workshop on Metrology for Industry 4.0 & IoT, Roma, Italy, pp. 407-412. https://doi.org/10.1109/MetroInd4.0IoT48571.2020.9138205

[13] Wang, X., Zscherpel, U., Tripicchio, P., D'Avella, S., Zhang, B., Wu, J., Yu, X. (2025). A comprehensive review of welding defect recognition from X-ray images. Journal of Manufacturing Processes, 140: 161-180. https://doi.org/10.1016/j.jmapro.2025.02.039

[14] Halfawy, M.R., Hengmeechai, J. (2014). Automated defect detection in sewer closed circuit television images

using histograms of oriented gradients and support vector machine. Automation in Construction, 43: 195-207. https://doi.org/10.1016/j.autcon.2013.10.012

[15] Wang, H., Fan, Z., Chen, X., Cheng, J., Chen, W., Wang, Z., Bu, Y. (2022). Automated classification of pipeline defects from ultrasonic phased array total focusing method imaging. Energies, 15(21): 8272. https://doi.org/10.3390/en15218272

[16] Kumaresan, S., Aultrin, K.J., Kumar, S.S., Anand, M.D. (2022). Deep learning based simple CNN weld defects classification using optimization technique. Russian Journal of Nondestructive Testing, 58(6): 499-509. https://doi.org/10.1134/S1061830922060109

[17] Valavanis, I., Kosmopoulos, D. (2010). Multiclass defect detection and classification in weld radiographic images using geometric and texture features. Expert Systems with Applications, 37(12): 7606-7614. https://doi.org/10.1016/j.eswa.2010.04.082

[18] Prakash, N., Srinivasan, V., Sharma, S. (2023). Learning defects from aircraft NDT data using HoG-Linear SVM classifier for minor flaw detection. NDT & E International, 138: 102885. https://doi.org/10.1016/j.ndteint.2023.102885

[19] Sasmito, B., Setiadji, B.H., Isnanto, R.R. (2025). Object detection: Real-time road damage detection and geolocation using YOLOv8 and GNSS integration. Ingénierie des Systèmes d'Information, 30(9): 2321-2329. https://doi.org/10.18280/isi.300909

[20] Ji, C., Wang, H., Li, H. (2023). Defects detection in weld joints based on visual attention and deep learning. NDT & E International, 133: 102764. https://doi.org/10.1016/j.ndteint.2022.102764

[21] Sakshi, Vijay, R., Lodhi, S., Noonia, A., Berar, G., Kumar, A. (2025). Encoder-decoder architectures for crack detection on surfaces: A deep learning approach. Ingénierie des Systèmes d'Information, 30(2): 495-503. https://doi.org/10.18280/isi.300221

[22] Yu, R., Guo, S., Huang, Y., Wang, L., Peng, Y., Wang, K. (2023). Measurement of weld penetration for variable-groove weldment using dual-band imaging and a neural network. Journal of Materials Research and Technology, 24: 2640-2652. https://doi.org/10.1016/j.jmrt.2023.03.183

[23] Srilatha, M., Srinivasu, N. (2024). Design an effective, faster region-based convolutional neural network with crow search optimization for the human tracking system. Journal of Electrical Systems, 20(6s): 1241-1256. https://doi.org/10.52783/jes.2853